IL NUOVO CIMENTO Vol. 24 C, N. 6 Novembre-Dicembre 2001

The role of extraterrestrial particles in the formation of the ozone hole(*)

Part I: The concentration of extraterrestrial particles at ozone hole formation

J. Rosinski(1)(**) and T. C. Kerrigan(2)(***)

(1) *Dipartimento di Fisica, Università di Ferrara - Via Paradiso 12, 44100 Ferrara, Italy*
(2) *Intel Corporation, EY2-E3 - 5200 N.E. Elam Young Parkway Hillsboro, OR, USA, 97124-6497*

(ricevuto il 19 Novembre 2000; revisionato il 28 Novembre 2000; approvato il 14 Febbraio 2001)

Summary. — The object of Part I of this paper is to estimate the concentration of extraterrestrial particles in the ozone layer over South Pole, Antarctica, during ozone hole formation. This estimate is based on an analysis of microscopic magnetic spherules collected in an extended program of atmospheric sampling. Spherules are shown to be of extraterrestrial origin and serve as markers for the larger class of less distinguished extraterrestrial particles. These particles settle to ground level as aggregates formed in a stratospheric ice crystal coalescence process. Specific spherule arrivals at ground level are strongly associated with apparent ozone depletion episodes during formation of the ozone hole. The origin of these spherules is a major stream of extraterrestrial particles independent of known meteor showers. The variability in its intensity from year to year corresponds to the variability in ozone depletion in the ozone hole itself. A quantitative theory based on these spherule arrivals and this coalescence process implies that the concentration of extraterrestrial particles at ozone hole formation lies between 500 and 2000 / m^3. A mechanism is proposed in Part II of this paper by which particle concentrations in this range are sufficient to produce the ozone hole.

PACS 92.60 – Meteorology.
PACS 94.10 – Physics of the neutral atmosphere.
PACS 94.10.Fa – Atmospheric composition (atomic or molecular), chemical reactions and processes.
PACS 82.33.Tb – Atmospheric chemistry.

(*) The authors of this paper have agreed to not receive the proofs for correction.
(**) E-mail: janros@earthlink.net
(***) E-mail: kerrigat@earthlink.net

1. – Introduction

In 1953, Bowen hypothesized a connection between certain meteor showers and subsequent statistically derived maximum rainfall days with a 28(±2) day delay [1]. Whipple and Hawkins showed that any such connection would depend on streams of micron-sized meteoritic particles accompanying these showers [2]. These particles would survive entry and settle through the atmosphere to act as ice forming nuclei in tropospheric precipitation processes. One of the principal criticisms of this hypothesis was lack of evidence for the existence of such particles.

In 1967, Rosinski began a series of experiments to determine their existence and any role they might play in the formation of precipitation [3]. Large volumes of air were sampled on a daily basis at stations widely dispersed over the globe. The sampled air was drawn through synthetic fiber filters suited to capturing such particles. Each filter was later dissolved in an inorganic solvent and magnetic particles were extracted from the solution with a magnet. These particles were then mounted and examined under an electron microscope. Photographs of six spherules are shown in fig. 1 [4].

Magnetic spherules (iron oxide spheres) were easily distinguished from other particles under this examination. They were regarded as potentially of extraterrestrial origin [5] and indeed might serve as markers for the larger class of less distinguished micrometeorites. Magnetic spherules were sized and counted for each sampling day and site for programs conducted in 1967, 1969, and 1971. Analysis of this data has led to the following general conclusions:

Magnetic spherules are of extraterrestrial origin (sect. **2**).

Magnetic spherules serve as markers for a potentially much larger class of extraterrestrial particles (sect. **3**).

Extraterrestrial particles are often assisted in settling through the atmosphere by incorporation into ice crystal aggregates (sect. **4**).

Magnetic spherules sampled at ground level need not be associated with known meteor showers (sect. **5**).

Extending this analysis, we find essentially no association between episodes of (apparent) ozone depletion during formation of the ozone hole and known meteor showers, but a strong association between these depletion episodes and certain specific spherule arrival episodes. Based on this association, we hypothesize the existence of a major stream of micrometeorites that furnishes particles to the ozone layer during formation of the ozone hole (sect. **6**). This stream is not associated with known meteor showers. It has a negative radiant declination and a slow speed of entry into the atmosphere. The variability in its intensity from year to year corresponds to the variability in ozone depletion in the ozone hole itself [6].

The object of Part I of this paper is to estimate the concentration of extraterrestrial particles in the ozone layer over South Pole, Antarctica, during ozone hole formation. Applying the coalescence theory derived in appendix A to the spherule arrival episodes associated with ozone depletion, we estimate this concentration to be between 500 and 2000 / m^3 (sect. **7**). We shall propose a mechanism in Part II of this paper by which extraterrestrial particle concentrations in this range are sufficient to actually produce the ozone hole.

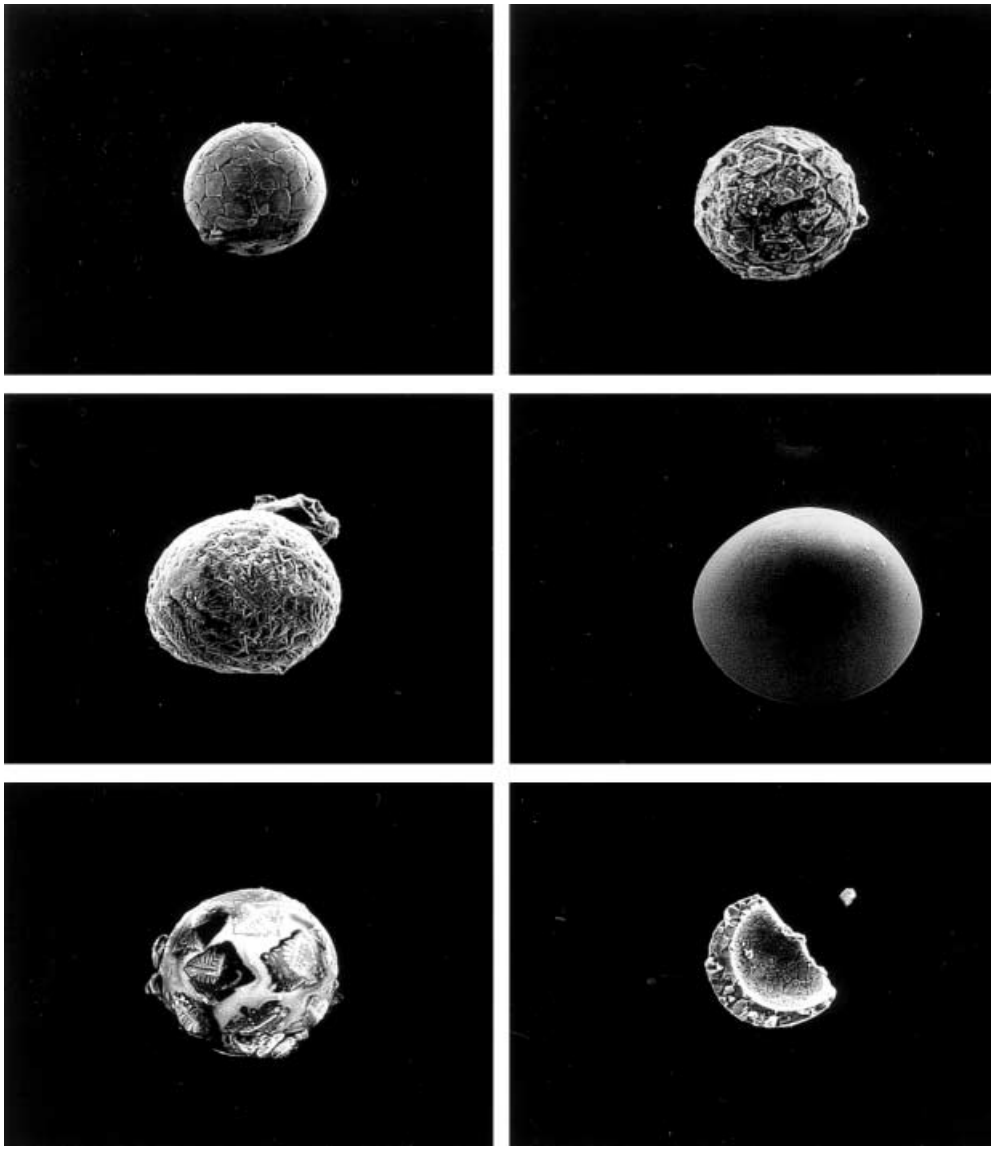

Fig. 1. – Scanning electron microscope photographs of five magnetic spherules and one spherule fragment. Diameters range from 15 to 20 μm. The photograph of the fragment shows that larger spherules may contain cavities.

2. – Extraterrestrial origin of magnetic spherules

Concentration peaks of magnetic spherules appear simultaneously at sampling stations widely dispersed over the globe. A particularly striking example is given in fig. 2. Magnetic spherule count (#/1000 m^3) *vs.* day of year is plotted for the period August 18-31, 1967, for four sampling stations: Mauna Loa, HI (19° N, 155° W), Boulder, CO

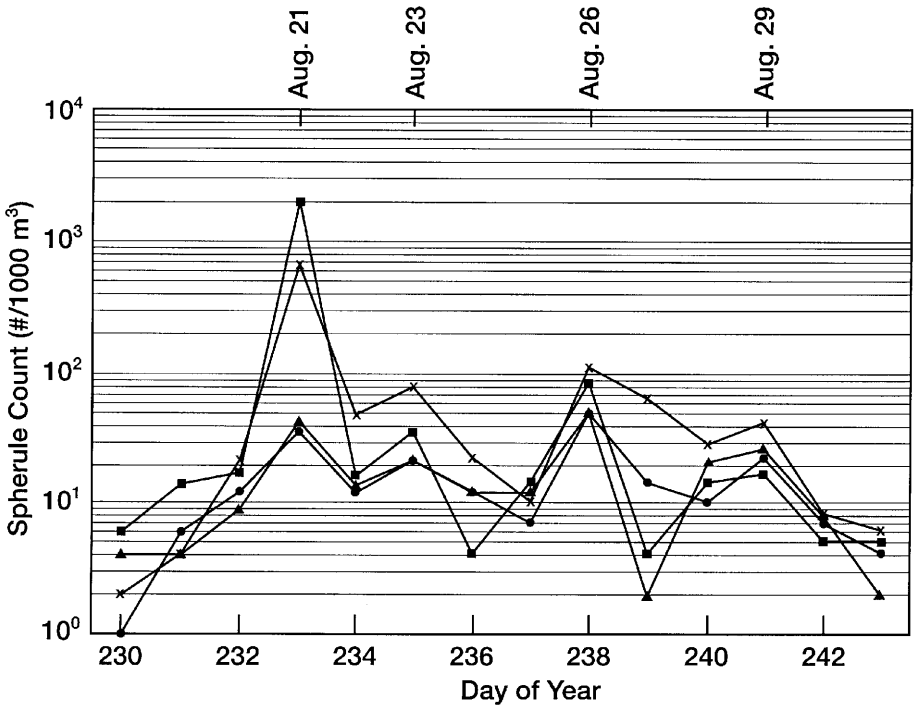

Fig. 2. – Magnetic spherule count *vs.* day of year for the period August 18-31, 1967, and four sampling stations (× College, AK; ▲ Bemidji, MN; ■ Boulder, CO; • Mauna Loa, HI).

(40° N, 105° W), Bemidji, MN (48° N, 95° W), and College, AK (64° N, 148° W) [3]. Each of the four concentration peaks occurs on the same day at all stations. (Times and date crossings are reckoned in GMT.) Given the large distances separating these stations and the simultaneity of these peaks on a 24 h time scale, local sources for these spherules

TABLE I. – *Ratios of magnetic particle count to magnetic spherule count and average magnetic particle radii for two sampling sites (Boulder, CO, and College, AK) and four days (1, 4, 6, 10 October, 1969).*

Day	Particle/Spherule ratio		Particle radius (μm)	
(October, 1969)	CO	AK	CO	AK
1	114	186	3.6	4.9
4	93	236	4.5	3.3
6	38	122	4.8	5.4
10	37	121	4.6	5.9
Average	70	166	4.4	4.9

are categorically excluded. Analysis of spherule size distributions, surface features, and elemental chemical composition confirms extraterrestrial origin.

3. – Spherules as extraterrestrial particle markers

Particle samples taken in 1969 at Boulder, CO, and College, AK, were subjected to two successive extractions [7]. The first was the usual extraction of magnetic spherules. The remaining particles were then subjected to the same extraction procedure but with a stronger magnet. The weakly magnetic particles obtained in this second extraction were also sized and counted. Table I gives the ratio of particle count to spherule count for the two sites and four days (average ratio = 118). Table I also gives the average radius (volumetric) for the magnetic particles for the same sites and days (average particle radius = 4.6 μm). Preliminary analysis of the occurrence of concentration peaks, size distributions, physical characteristics, and elemental chemical composition strongly suggests that this larger class of weakly magnetic particles is also of extraterrestrial origin.

Large concentrations of non-magnetic and slightly magnetic glassy spheroids were incidentally observed in several samples collected in October, 1971 [4]. These particles were up to 100 times more numerous than the magnetic spherules in the same samples. The average chemical composition (% atoms by ion etch) for the 16 spheroids analyzed was 55.7% oxygen, 19.4% silicon, 9.8% aluminum, 4.3% iron, 2.7% titanium, 2.4% barium, 1.6% calcium, ... Nickel, manganese, chromium, and titanium were present in each of the spheroids. Their concentrations were up to 20 times higher in the subsurface than at the surface. The presence of these elements strongly suggests extraterrestrial origin for these particles. The distribution of these elements relative to spheroid surfaces strongly suggests their fractionation during particle entry into the atmosphere.

Extraterrestrial particles undergo brief but rapid heating as they enter the atmosphere. Magnetic spherules and glassy spheroids are evidently formed when such particles are heated to the melting point. Although magnetic spherules do indeed constitute a marker for the general class of extraterrestrial particles, estimating the concentration of these particles from spherule counts is problematical. Extraterrestrial particles generally form a small fraction of the sampled aerosol population, and extraterrestrial and terrestrial particles are fundamentally difficult to distinguish. The fraction of magnetic spherules at ground level depends on the mix of metal and non-metal particles in a stream before entry into the atmosphere. This fraction also depends on speeds and angles of entry of particles into the atmosphere [8, 9]. Slower speeds or more shallow angles of entry result in less heating and so relatively fewer spherules. Further, non-metal and mixed-composition particles tend to melt at higher temperatures. Despite these difficulties, the analyses cited here indicate that both metal and non-metal particles can be on the order of 100 times more numerous than magnetic spherules.

Finally, we note that particle densities vary widely. Magnetic spherules consist primarily of iron oxides, so the smallest spherules may have densities as high as 5.5 g/cm^3. Larger magnetic spherules generally contain a spherical cavity (fig. 1), so their effective densities can be as low as 1.1 g/cm^3 [10]. Weakly magnetic particles also consist primarily of iron oxides. Glassy spheroids and unfused non-metallic particles consist primarily of aluminum silicates and generally have densities less than 3.0 g/cm^3. For specificity, we take the average for the entire population to be 3.5 g/cm^3.

4. – Assisted settling of extraterrestrial particles

The terminal velocity for a (spherical) particle falling in air is given by an empirical extension of Stokes' formula [11]:

$$v = \frac{2\rho\tilde{g}r^2}{9\mu}\left(1 + A(\lambda/r) + Q(\lambda/r)e^{-br/\lambda}\right),$$

where

v is the particle terminal velocity (cm/s),

ρ is the effective particle density (g/cm^3),

$\tilde{g}$ is the gravitational acceleration ($\sim$980 cm/s^2),

r is the effective particle radius (cm),

μ is the dynamic viscosity of air (g/cm/s),

λ is the mean free path of air molecules (cm),

$A = 0.77$,

$Q = 0.40$,

$b = 1.62$.

A, Q, and b are empirically determined dimensionless constants. The values given here are for glass spheres falling in air.

According to this formula, unassisted aerodynamic settling to ground level takes $\sim$62 days for 2.5 μm radius spherules (5.5 g/cm^3) and $\sim$19 days for 12.5 μm radius spherules (1.1 g/cm^3). These predictions conflict diametrically with sampling data:

– Unassisted settling would tend to extend an arrival episode's duration by 43 days. Spherule arrival episodes actually last 10 to 20 days, a time span comparable to the duration of visible meteor showers and presumably also of extraterrestrial particle streams (see table III).

– Unassisted settling would inadvertently sort extraterrestrial particles by size (radius and density): 12.5 μm spherules in any given stream would arrive at ground level 43 days earlier than 2.5 μm spherules. However, spherules in any given daily sample generally vary widely in size [3].

– Correlations in spherule concentration fluctuations between sampling stations (fig. 2) cannot be produced by tropospheric cloud physical processes. These processes are local and so the fluctuations they produce would be uncorrelated.

To resolve these conflicts, we propose a mechanism in which extraterrestrial particles sampled at ground level settle through most of the atmosphere as aggregates (appendix A). In particular, particles settle individually to about 30 km altitude. Settling slows appreciably between 20 and 30 km. Particle concentrations increase proportionately. Absorption of solar radiation by ozone in this layer causes the air temperature to cycle diurnally [12]. (North and South Pole are immune to this cycling since the sun rises

and sets on the poles just once each year.) During intervals of lowest temperature, water vapor density exceeds saturation. Extraterrestrial particles act as ice forming nuclei and capture excess water vapor to produce ice crystals. This population evolves according to the coalescence equation [13]. Ice crystal aggregates that grow beyond a critical size precipitate out of this layer. During their descent from 20 to 10 km, the ice sublimates to yield loosely bound particle aggregates. The resolution of features in fig. 2 implies the descent of particle aggregates from 10 to 0 km takes on the order of 24 h.

Spherules that do not make a rapid descent to ground level in aggregates are susceptible to capture by tropospheric precipitation processes [14, 4]. Particle aggregates have been observed on rare occasions, but are almost certainly broken up in laboratory processing [3]. Sampling has not been isokinetic, so sampling efficiency for large particles, including aggregates, is unknown; spherule concentrations may be significantly underestimated.

Ice crystal coalescence is a complex, non-stationary, non-linear process. The theory developed in appendix A treats only its grossest features. The formation of precipitation requires specific combinations of particle concentrations, temperature fluctuations, and water vapor densities. The precipitation itself depletes particles and water vapor and may induce its own cessation. Such a precipitation cycle would repeat when these quantities are replenished. The result may be pulsations in spherule concentrations at ground level difficult to distinguish from variations produced by variations in the influx of particles at the top of the atmosphere or scavenging by precipitation processes in the troposphere.

Despite these ambiguities, key features in the data support this theory. The most notable is the occurrence of bimodal magnetic spherule size distributions [14]. These distributions are characteristic of coalescence processes in general. Contrary to the simplification assumed in appendix A, ice crystal size at the start of coalescence generally varies directly with particle size. Since the largest crystals preferentially scavenge the smallest crystals, the particle residues of precipitating ice crystal aggregates tend to consist of the largest and the smallest particles. Hence, the bimodal spherule size distributions. Further consideration of these points lies beyond the scope of this paper.

5. – Meteor shower association with spherule arrivals

The object of this section is to analyze the extent to which visible meteor showers may be associated with magnetic spherule arrival episodes. A strong association based on an 11 day assisted settling time would lend support to the coalescence theory of sect. **4**. It would also shed light on the relation between meteor showers and particle streams in general. Clarification of these two issues will help to sharpen the estimates of extraterrestrial particle concentrations at ozone hole formation derived in sect. **7**.

The first two steps in this analysis consist of simply listing specific spherule arrival episodes and candidate meteor showers. The next two steps consist of specifying the general temporal and spatial relations between arrival episodes and meteor showers. The final step consists of assessing the likelihood that a given candidate shower is related in time and space to a given arrival episode. In particular, it is an assessment of the likelihood that a potential particle stream corresponding to a given visible meteor shower can make a significant contribution to the spherule count of the arrival episode.

This assessment shows that a significant number of spherule arrival episodes have closely associated meteor showers. However, it also shows that not all meteor showers have corresponding particle streams, and not all particle streams have corresponding meteor showers.

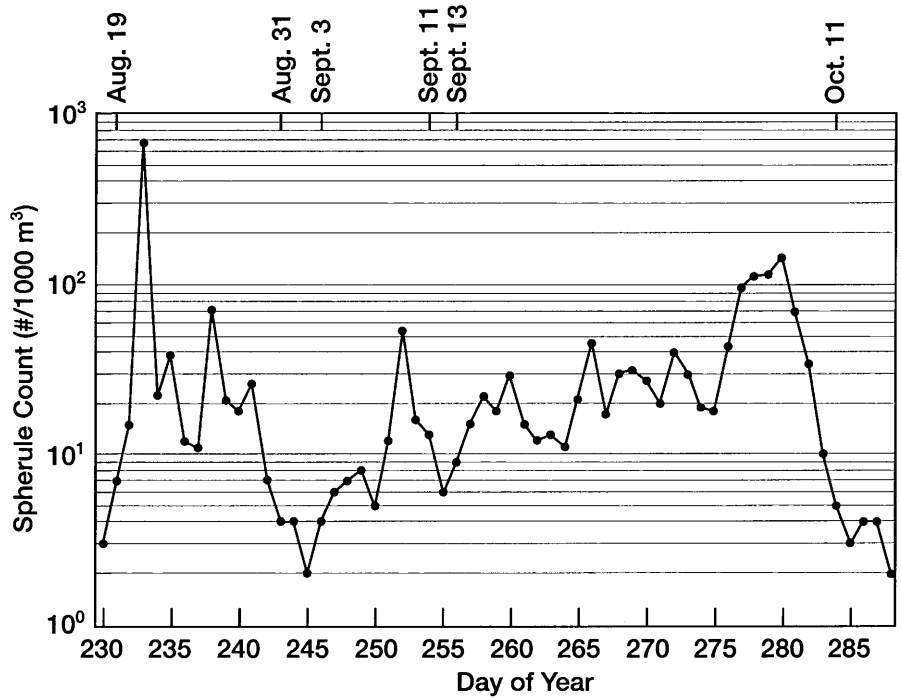

Fig. 3. – Magnetic spherule count *vs.* day of year averaged over five sampling stations for the period August 18-October 15, 1967.

Magnetic spherule arrival episodes.

The most detailed published data for the magnetic spherule sampling program spans August 18-October 15, 1967, for stations at College, AK, Bemidji, MN, Boulder, CO, Mauna Loa, HI, and Kericho, Kenya (1° S, 36° E) [3]. The graph of average magnetic spherule count (#/1000 m^3) *vs.* day of year for these five stations is given in fig. 3. Inspection of this data in detail indicates three distinctive spherule arrival intervals: Aug. 19-Aug. 31, Sept. 3-Sept. 11, and Sept. 13-Oct. 11.

Magnetic spherule sampling data is also given for October 1967, 1969, and, 1971 at three Southern Hemisphere sampling sites: Kericho, Kenya, Rustenberg, Republic of South Africa (26° S, 27° E), and Christchurch, New Zealand (43° S, 172° E) [6]. Results for South Africa and New Zealand are available for 1969; results for Kenya are available for 1967 and 1971. Three spherule arrival intervals are evident: I: Oct. 1-Oct. 13, II: Oct. 15-Oct. 24, and III: Oct. 25-Nov. 3. Spherules were detected in Interval I for all available times and dates. Virtually no spherules were detected in Interval II in Kenya in 1967, or in either South Africa or New Zealand in 1969; however, spherules were detected in Interval II in Kenya in 1971. Finally, spherules were detected in Interval III in Kenya but not in South Africa or New Zealand. These observations are summarized in table II.

Candidate meteor showers.

A list of known meteor showers (July through October) is given in table III [15]. The table includes shower dates, date of maximum shower activity, average speed of

TABLE II. – *Magnetic spherule arrival episodes and corresponding time intervals (I: Oct. 1-Oct. 13, II: Oct. 15-Oct. 24, III: Oct. 25-Nov. 3) for three years and three sampling sites.*

Sampling Site	1967	1969	1971
Kenya	I, III	(no data)	I, II, III
South Africa	(no data)	I	(no data)
New Zealand	(no data)	I	(no data)

TABLE III. – *A list of known meteor showers (July through October) including shower dates, date of maximum shower activity, average speed of atmospheric entry, shower rating (strength and reliability), and shower radiant declination.*

Shower	Dates	Date (max)	Speed (km/s)	Rating	Declination (°)
July Pegasids	07/07-13/07	10/07	70	II	+15
July Phoenicids	10/07-16/07	13/07	47	III	−48
Alpha Cygnids	11/07-30/07	18/07	37	IV	+47
Sigma Capricornids	15/07-11/08	20/07	30	IV	−15
Pices Austrinids	15/07-10/08	28/07	35	II	−30
South Delta Aquarids	12/07-19/08	28/07	41	I	−16
Alpha Capricornids	03/07-15/08	30/07	23	II	−10
South Iota Aquarids	25/07-15/08	04/08	34	II	−15
North Delta Aquarids	15/07-25/08	08/08	42	II	−05
Perseids	17/07-24/08	12/08	59	I	+58
Kappa Cygnids	03/08-25/08	17/08	25	II	+59
North Iota Aquarids	11/08-31/08	20/08	31	II	−06
Pi Eridanids	20/08-05/09	25/08	59	IV	−15
Gamma Doradids	19/08-06/09	28/08	41	IV	−50
Alpha Aurigids	25/08-05/09	01/09	66	II	+42
September Perseids	05/09-10/10	08/09	64	II	+47
Aries-Triangulids	09/09-16/09	12/09	35	IV	+29
Piscids	01/09-30/09	20/09	26	II	00
Kappa Aquarids	08/09-30/09	20/09	16	IV	−02
October Arietids	01/10-31/10	08/10	28	I	+08
Giacobinids	06/10-10/10	08/10	20	III	+54
Delta Aurigids	22/09-23/10	10/10	64	II	+52
Epsilon Geminids	14/10-27/10	18/10	71	II	+27
Orionids	02/10-07/11	21/10	66	I	+16
Leo Minorids	21/10-23/10	22/10	62	IV	+37

atmospheric entry, shower rating, and shower radiant declination. Rating is a measure of a shower's strength and reliability:

i) the strongest annual showers with ZHRs (Zenith Hourly Rate) above 10 at maximum activity,

ii) dependable minor showers with ZHRs of at least 3 at maximum activity,

iii) showers with irregular rates ranging from nil to strong,

iv) minor showers that are difficult to distinguish from sporadic background.

Radiant declination is the angle between the meteor shower's velocity vector and the Earth's equitorial plane. Showers with positive radiant declinations are "northern"; those with negative declinations are "southern".

Temporal relation between meteor showers and arrival episodes.

Extraterrestrial particle streams provide the link between visible meteor showers and spherule arrival episodes. The nature of these streams is difficult to infer. Since atmospheric entry does not produce visible meteors, the strength, the variability, and the dates of a stream are unknown. Strength and variability may be revealed in spherule data. Our working hypothesis is that dates for meteor showers and corresponding particle streams coincide.

The time for a particle of radius 5 μm and density 3.5 g/cm^3 to settle to 25 km altitude is $\sim$10 days. Given the coalescence theory advanced in sect. **4**, aggregates of these particles arrive at ground level $\sim$11 days after atmospheric entry of the originating particle stream. By translating the time interval for a spherule arrival episode by 11 days, we will have projected dates for meteor showers corresponding to the episode.

The translated intervals for the arrival episodes corresponding to fig. 3 are Aug. 8-Aug. 20, Aug. 23-Aug. 31, and Sept. 2-Sept. 30. The translated intervals corresponding to table II are Sept. 20-Oct. 2, Oct. 4-Oct. 13, and Oct. 14-Oct. 23.

Spatial relation between meteor showers and arrival episodes.

The spatial relation between a meteor shower and a spherule arrival episode is equal to that between an associated particle stream and the arrival episode. For this analysis, this relation is characterized by relative (extraterrestrial particle) flux. Relative flux is a measure of the dependence of spherule count at a given sampling station on the latitude of the station, and the speed and declination of a particle stream contributing to the count. Unfortunately, this metric fails to account for the dependence of particle ablation on angle of entry into the atmosphere or the modulation of spherule counts by precipitation processes.

Let $\vec{R}$ denote the position vector for a sampling station and $\vec{V}$ the velocity vector for an extraterrestrial particle stream. Appendix B derives an analytical estimate for the instantaneous particle flux $F(\theta, V)$ over the sampling station as a function of θ, the angle between $\vec{R}$ and $-\vec{V}$, and V, the magnitude of $\vec{V}$. The relative instantaneous flux RF is just the absolute instantaneous flux over the sampling station divided by the maximum absolute instantaneous flux taken over the surface of the Earth, $F(\theta, V)/F(0, V)$. In the limit of large V, where particle orbits are essentially linear, $RF(\theta, V) = \cos\theta$. Appendix B shows that for slower streams the gravitational lens effect is significant and RF is a much more complicated function of θ and V.

To account for the dependence of $\vec{R}$ on time, take a coordinate system in which $\vec{R}$ and $\vec{V}$ have representations

$$\vec{R}(t) = (R\cos\lambda\cos\omega t, R\cos\lambda\sin\omega t, R\sin\lambda)$$

and

$$\vec{V} = -(V\cos\delta, 0, V\sin\delta),$$

where

R is the radius of the Earth (plus atmosphere), 6.37×10^8 cm,

λ is the latitude of the sampling station (radians),

ω is the angular velocity of the Earth (radians/s),

t is time (s),

V is the magnitude of $\vec{V}$(cm/s),

δ is the radiant declination of the particle stream (radians).

Then RF over the sampling station depends on time through the relation

$$\cos\theta(t) = \frac{-\vec{V}\cdot\vec{R}(t)}{VR} = \cos\delta\cos\lambda\cos\omega t + \sin\delta\sin\lambda.$$

Relative flux $\overline{RF}(\lambda, \delta, V)$ is simply $RF(\theta(t), V)$ averaged over a 24 h period T:

$$\overline{RF}(\lambda, \delta, V) \equiv \frac{1}{T}\int_0^T RF(\theta(t), V)\mathrm{d}t.$$

The integrand is taken to be zero when the sampling station is in the shadow of the Earth. $\overline{RF}$ attains its maximum value of 1 for two special cases: $\lambda = \delta = \pm 90°$. Sample calculations of $\overline{RF}$ *vs.* λ for $V = 20$ km/s and four values of δ (0°, −20°, −40°, −60°) are given in fig. 4. They show in particular how radiant declination of a slow shower affects $\overline{RF}$ at South Pole, the point on the Earth where $\overline{RF}$ achieves its maximum in three of the four cases considered.

Association between meteor showers and arrival episodes.

The association between magnetic spherule arrival episodes for fig. 3 and known meteor showers listed in table III is summarized in table IV. A brief analysis of candidate showers is provided for each episode. The likelihood that a shower contributes to the given episode is assessed on the basis of shower dates, date of maximum activity, shower speed and ranking, and relative flux at four sampling stations. The most likely showers are highlighted.

Translated Arrival Interval Aug. 8-Aug. 20: South Iota Aquarids is excluded as a likely candidate. Its shower dates and its date of maximum activity are both misaligned with the translated event dates. Further, relative flux falls off to lower levels at higher

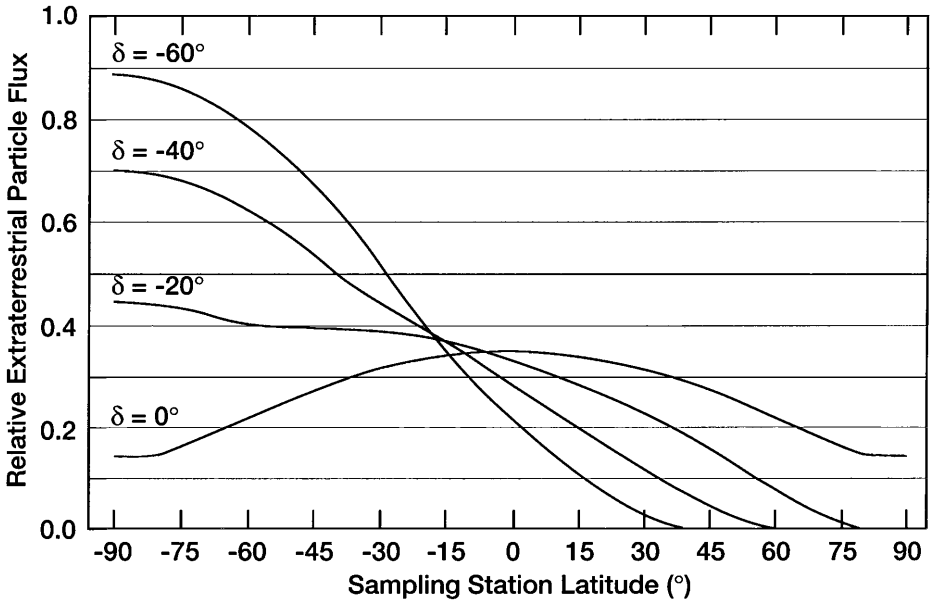

Fig. 4. – Relative extraterrestrial particle flux *vs.* sampling station latitude for four values of particle stream radiant declination ($\delta = 0°$, $-20°$, $-40°$, $-60°$).

TABLE IV. – *A table showing temporal and spatial relations between magnetic spherule arrival episodes and candidate meteor showers. The "Event Dates" are translates of dates for episodes shown in fig.* 3. *"Date (max)" denotes date of maximum shower activity. "Speed" denotes speed of atmospheric entry. "Rating" denotes shower rating for strength and reliability. "Relative flux" denotes estimated relative flux of extraterrestrial particles above sampling stations at latitudes* $\lambda = 19°/40°/48°/64°$. *Highlighted candidates are regarded as the most likely magnetic spherule sources.*

Event dates (translated)	Shower	Shower dates	Date (max)	Speed (km/s)	Rating	Relative flux
8 Aug.-	South Iota Aquarids	25/7-15/8	4/8	34	II	0.26/0.17/0.13/0.05
20 Aug.	**North Delta Aquarids**	15/7-25/8	8/8	42	II	0.29/0.22/0.19/0.11
	Perseids	17/7-24/8	12/8	59	I	0.32/0.55/0.63/0.77
	Kappa Cygnids	3/8-25/8	17/8	25	II	0.36/0.59/0.67/0.79
	North Iota Aquarids	11/8-31/8	20/8	31	II	0.29/0.22/0.19/0.11
23 Aug.-	North Iota Aquarids	11/8-31/8	20/8	31	II	0.29/0.22/0.19/0.11
31 Aug.	Pi Eridanids	20/8- 5/9	25/8	59	IV	0.25/0.16/0.12/0.04
	Gamma Doradids	19/8- 6/9	28/8	41	IV	0.09/0.00/0.00/0.00
	Alpha Aurigids	25/8- 5/9	1/9	66	II	0.34/0.45/0.50/0.60
2 Sept.-	**September Perseids**	5/9-10/10	8/9	64	II	0.34/0.47/0.54/0.66
30 Sept.	**Aries-Triangulids**	9/9-16/9	12/9	35	IV	0.36/0.40/0.41/0.45
	Piscids	1/9-30/9	20/9	26	II	0.32/0.27/0.24/0.17
	Kappa Aquarids	8/9-30/9	20/9	16	IV	0.36/0.32/0.29/0.24

latitudes, a trend not indicated in fig. 2. North Delta Aquarids is included even though it is a faster shower with a marginal fall-off in relative flux. Its date of maximum activity (Aug. 8) lies close to the translated concentration spike for this arrival episode (Aug. 10). Perseids is provisionally included as a likely candidate. It qualifies on the basis of dates and relative flux profile. Although it is a fast shower, the Earth's rotation may provide a significant fraction of particles with a shallow enough entry angle to survive ablation. Kappa Cygnids qualifies as a likely candidate by all criteria. Note also that the dates of maximum activity for Perseids and Kappa Cygnids (Aug. 12 and 17) lie close to the two translated concentration peaks for this arrival episode (Aug. 10 and 15). North Iota Aquarids is excluded because of misaligned dates and a marginal fall-off in relative flux. (Neither point by itself is exclusionary.) South Iota Aquarids and North Iota Aquarids appear to be meteor showers without corresponding particle streams.

Translated Arrival Interval Aug. 23-Aug. 31: North Iota Aquarids is excluded as a likely candidate since its date of maximum activity (Aug. 20) precedes the (translated) concentration spike for this arrival episode (Aug. 29) by nine days. Pi Eridanids and Gamma Doradids are both excluded since relative flux decreases rapidly with increasing latitude. Alpha Aurigids is provisionally included. Its date of maximum activity (Sept. 1) follows the translated concentration spike (Aug. 29) by just two days. However, it is an extremely fast shower and the fraction of particles surviving entry into the atmosphere is probably small.

Translated Arrival Interval Sept. 2-Sept. 30: This episode spans the entire month of September and is most likely produced by multiple streams. Judging by the dates of maximum shower activity, September Perseids and Aries-Triangulids contribute to the first half and Piscids and Kappa Aquarids contribute to the second half of the episode. In particular, the spherule concentration peaks on Sept. 17 and Sept. 23 translate to Sept. 6 and Sept. 12. The dates for maximum activity for September Perseids and Aries-Triangulids are Sept 8 and Sept. 12. Likewise, the spherule concentration peaks on Sept. 29 and Oct. 7 translate to Sept. 18 and Sept. 26. The dates for maximum activity for Piscids and Kappa Aquarids are both Sept. 20. September Perseids is included only provisionally because of speed.

The association between magnetic spherule arrival episodes for table II and known meteor showers listed in table III is summarized in table V.

Translated Arrival Interval Sept. 20-Oct. 2: Piscids and Kappa Aquarids are included as likely candidates even though their dates of maximum activity occur at the start of the translated arrival interval.

Translated Arrival Interval Oct. 4-Oct. 13: October Arietids is excluded as a likely candidate precisely because it appears to be such a strong candidate for all the years and sites indicated in table II. However, magnetic spherules were not detected in significant numbers in this arrival interval except in Kenya in 1971. October Arietids is evidently a shower without an associated particle stream. The relative flux profiles show that both Giacobinids and Delta Aurigids may contribute in Kenya but not in South Africa or New Zealand. Delta Aurigids is excluded, however, because it has rating I and so should have contributed in Kenya for both 1967 and 1971 if it were to contribute at all. Giacobinids is the sole likely candidate. Its declination explains its lack of contribution in South Africa and New Zealand, and its rating of III explains its lack of contribution in Kenya in 1967.

Translated Arrival Interval Oct. 14-Oct. 23: October Arietids and Orionids are excluded as likely candidates. Their relative flux profiles imply contributions to magnetic spherule counts in South Africa and New Zealand; in fact, none was observed. The remaining showers are also unlikely to contribute. All are fast. The relative flux profile

TABLE V. – *A table showing temporal and spatial relations between magnetic spherule arrival episodes and candidate meteor showers. The "Event Dates" are translates of dates for episodes given in table II. "Date (max)" denotes date of maximum shower activity. "Speed" denotes speed of atmospheric entry. "Rating" denotes shower rating for strength and reliability. "Relative flux" denotes estimated relative flux of extraterrestrial particles above sampling stations at latitudes* $\lambda = -1^\circ / -26^\circ / -43^\circ$. *Highlighted candidates are regarded as the most likely magnetic spherule sources.*

Event dates (translates)	Shower	Shower dates	Date (max)	Speed (km/s)	Rating	Relative flux
20 Sept.-	**Piscids**	01/09-30/09	20/09	26	II	0.33/0.30/0.26
2 Ott.	**Kappa Aquarids**	08/09-30/09	20/09	16	IV	0.38/0.36/0.33
4 Ott.-	October Arietids	01/10-31/10	08/10	28	I	0.33/0.27/0.20
13 Ott.	**Giacobinids**	06/10-10/10	08/10	20	III	0.23/0.07/0.00
	Delta Aurigids	22/09-23/10	10/10	64	II	0.19/0.04/0.00
14 Ott.-	October Arietids	01/10-31/10	08/10	28	I	0.33/0.27/0.20
23 Ott.	Delta Aurigids	22/09-23/10	10/10	64	II	0.19/0.04/0.00
	Epsilon Geminids	14/10-27/10	18/10	71	II	0.28/0.16/0.07
	Orionids	02/10-07/11	21/10	66	I	0.30/0.22/0.14
	Leo Minorids	21/10-23/10	22/10	62	IV	0.25/0.11/0.03

for Epsilon Geminids implies a potential contribution at South Africa and New Zealand. The duration of Leo Minorids is extremely short and its date of maximum activity comes at the end of the arrival interval, and the date for maximum activity for Delta Aurigids is outside the interval altogether.

To summarize, the highlighted showers in tables IV and V were found to have close temporal and spatial associations with specific concentration peaks in spherule arrival episodes. These associations lend additional support to the coalescence theory advanced in sect. **4**. The remaining showers were found not to be associated with spherule arrival episodes. This lack of association supports the conclusion that not all meteor showers have corresponding particle streams. Further, two arrival episodes (Aug. 23-Aug. 31, table IV, and Oct. 14-Oct. 23, table V) are not substantially associated with any visible meteor showers. This lack of association supports the conclusion that not all particle streams have corresponding meteor showers.

6. – Meteor shower association with the ozone hole

The object of this section is to analyze the extent to which (apparent) ozone depletion episodes during formation of the ozone hole may be associated with either visible meteor showers or extraterrestrial particle streams. We find almost no association between depletion episodes and meteor showers, but a strong association between depletion episodes and spherule arrival episodes. This association forms the basis for estimating extraterrestrial particle concentrations at ozone hole formation in sect. **7**.

A graph of ozone mass *vs.* day of year is given in fig. 5 [16]. Ozone mass is taken to be the total mass of ozone (Dobson units) in a vertical column of unit cross-sectional

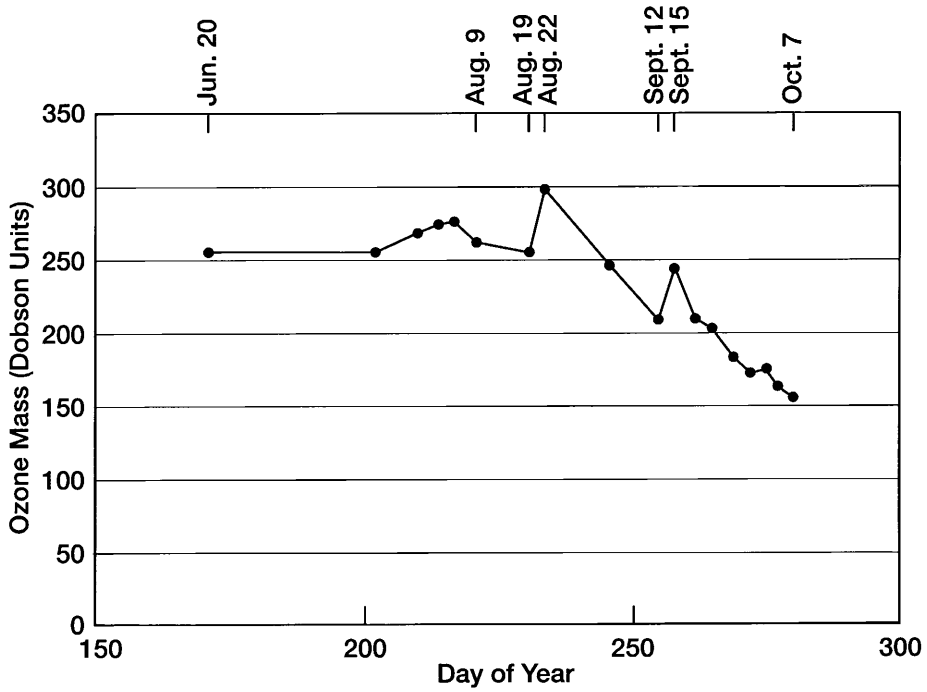

Fig. 5. – Total ozone mass in a standard column over south pole *vs.* day of year for the period June 19-October 7, 1986.

area extending from the bottom to the top of the atmosphere over South Pole. The time span (June 20-October 7, 1986) includes ozone hole formation. The ozone depletion episodes have approximate dates Aug. 9-Aug. 19, Aug. 22-Sept. 12, and Sept. 15-Oct. 7+. Settling of extraterrestrial particles should be unassisted since the diurnal temperature cycling that drives particle aggregation does not occur over South Pole. The time for an extraterrestrial particle of radius 5 μm and density 3.5 g/cm^3 to settle to 19 km, the altitude of peak ozone concentration over South Pole, is $\sim$14 days. The 14-day translates of these depletion intervals are July 26-Aug. 5, Aug. 8-Aug. 29, and Sept. 1-Sept. 23+.

The potential association between these ozone depletion episodes and known meteor showers listed in table III is summarized in table VI. A brief analysis of candidate showers is provided for each episode. The likelihood that a shower contributes to a depletion episode is assessed on the basis of shower dates, date of maximum activity, shower speed and ranking, and relative flux at South Pole. The most likely showers are highlighted.

Translated Depletion Interval July 26-Aug. 5: South Iota Aquarids was judged in sect. **5** not to have a corresponding particle stream and so is also excluded in this analysis. The remaining four showers appear to be likely candidates. If extraterrestrial particles are responsible for formation of the ozone hole, then this many likely candidates sets the expectation for formation during this interval. Although ozone concentration does dip during this interval, overall ozone concentration achieves its maximum just after this dip (Aug. 22). Reasons for both the dip and the general wintertime increase are not immediately clear. We address these issues in Part II of this paper.

TABLE VI. – *A table showing temporal and spatial relations between ozone depletion episodes and candidate meteor showers. The "Event dates" are translates of dates for episodes shown in fig.* 5. *"Date (max)" denotes date of maximum shower activity. "Speed" denotes speed of atmospheric entry. "Rating" denotes shower rating for strength and reliability. "Relative flux" denotes estimated relative flux of extraterrestrial particles above South Pole ($\lambda = -90^\circ$). Highlighted candidates are regarded as the most likely magnetic spherule sources.*

Event dates (translated)	Shower	Shower dates	Date (max)	Speed (km/s)	Rating	Relative flux
26 Jul.-	**Sigma Capricornids**	15/7-11/8	20/7	30	IV	0.30
5 Aug.	**Pices Austrinids**	15/7-10/8	28/7	35	II	0.52
	South Delta Aquarids	12/7-19/8	28/7	41	I	0.30
	Alpha Capricornids	3/7-15/8	30/7	23	II	0.27
	South Iota Aquarids	25/7-15/8	4/8	34	II	0.29
8 Aug.-	**North Delta Aquarids**	15/7-25/8	8/8	42	II	0.08
29 Aug.	Perseids	17/7-24/8	12/8	59	I	0.00
	Kappa Cygnids	3/8-25/8	17/8	25	II	0.00
	North Iota Aquarids	11/8-31/8	20/8	31	II	0.15
	Pi Eridanids	20/8- 5/9	25/8	59	IV	0.26
	Gamma Doradids	19/8- 6/9	28/8	41	IV	0.77
	Alpha Aurigids	25/8- 5/9	1/9	66	II	0.00
1 Sept.-	September Perseids	5/9-10/10	8/9	64	II	0.00
23+ Sept.	Aries-Triangulids	9/9-16/9	12/9	35	IV	0.00
	Piscids	1/9-30/9	20/9	26	II	0.05
	Kappa Aquarids	8/9-30/9	20/9	16	IV	0.28

Translated Depletion Interval Aug. 8-Aug. 29: North Delta Aquarids is included even though its value of relative flux is less than 10%. Recall that this shower was associated with the spike in the first arrival episode in fig. 3. Perseids, Kappa Cygnids, and Alpha Aurigids are excluded for zero relative flux. North Iota Aquarids, Pi Eridanids, and Gamma Doradids were judged in sect. **5** not to have corresponding particle streams.

Translated Depletion Interval Sept. 1-Sept. 23+: September Perseids, Aries-Triangulids, and Piscids are excluded for insufficient relative flux. Kappa Aquarids is included as a likely candidate.

To summarize, there is an abundance of likely candidates prior to the start of ozone hole formation. In particular, four out of the five showers corresponding to the Depletion Interval July 26-Aug. 5 are regarded as likely candidates. There is a dearth of likely candidate showers during ozone hole formation. In particular, North Delta Aquarids, the only likely candidate for the Depletion Interval Aug. 8-Aug. 29, has relative flux 0.08, and Kappa Aquarids, the only likely candidate for the Depletion Interval Sept. 1-Sept. 23+, has date of maximum activity 20 days after the start of this interval. A connection between visible meteor showers and formation of the ozone hole is unsupported by this analysis.

However, we also note that the magnetic spherule data presented in this paper is strongly suggestive of high concentrations of extraterrestrial particles in the ozone layer over South Pole precisely at ozone hole formation. Indeed, recall that the spherule arrival episodes associated with fig. 3 have dates Aug. 19-Aug. 31, Sept. 3-Sept. 11,

and Sept. 13-Oct. 11. Based on a 24 h assisted transport from 25 to 0 km and a 3-day unassisted settling time from 25 to 19 km for particles of radius 5 μm and density 3.5 g/cm^3, we translate these intervals by two days to project the time intervals in which the corresponding extraterrestrial particles are present over South Pole at 19 km. The translated intervals are Aug. 21-Sept. 2, Sept. 5-Sept. 13, and Sept. 15-Oct. 13. Given this translation, we note

– The first ozone depletion interval (Aug. 9-Aug. 19) precedes the time interval in which the ozone hole appears to form and also the time interval for which spherule data are available.

– The union of the first two intervals during which spherules are projected at 19 km (Aug. 21-Sept. 2 and Sept. 5-Sept. 13) coincides almost exactly with the first ozone depletion interval during ozone hole formation (Aug. 22-Sept. 12).

– The third interval during which spherules are projected at 19 km (Sept. 15-Oct. 13) coincides with the second ozone depletion interval during ozone hole formation (Sept. 15-Oct. 7+).

These coincidences provide additional support for the coalescence theory of sect. **4** and evidence for a relation between extraterrestrial particles and ozone hole formation.

7. – Particle concentrations at ozone hole formation

The object of this section is to estimate the concentration of extraterrestrial particles in the ozone layer over South Pole during ozone hole formation.

This estimate is based on the assisted settling mechanism proposed in sect. **4** and developed in mathematical detail in appendix A. The key observation is that the smallest extraterrestrial particle aggregate produced by this process settles from 10 to 0 km in about 24 hours. The terminal velocity is then about 11.6 cm/s. Given extraterrestrial particles with average radii 5 μm, densities 3.5 g/cm^3, and aggregate densities 3.0 g/cm^3, we compute the effective aggregate radius and so n_{prt}, the expected number of particles in the particle aggregates. The corresponding ice crystal aggregate mass is then $L = n_{\mathrm{prt}}(W/N)$, where W denotes water (g/cm^3) available for ice crystal growth, and N denotes number density (#/cm^3) of extraterrestrial particles in the coalescence layer.

The coalescence equation is then solved for the size distribution g, where $g(u)\delta u$ denotes the number density (#/cm^3) of precipitating ice crystal aggregates with mass in the interval $[u, u + \delta u]$, $u \geqslant L$. Finally, the expected number of magnetic spherules in a daily sample is given by the integral

$$n_{\mathrm{sph}} = \frac{V_{\mathrm{smp}} D_{\mathrm{C}} N}{8.64 \times 10^4 r_{\mathrm{ps}} W} \int_L^\infty \frac{u g(u)}{V_{\mathrm{agg}}(R_{\mathrm{agg}}(u))} \mathrm{d}u\,,$$

where

V_{smp} is the spherule sampling volume (10^9 cm^3),

D_{C} is the thickness of the ice crystal coalescence layer (10^6 cm),

r_{ps} is the ratio of the number of extraterrestrial particles to the number of magnetic spherules,

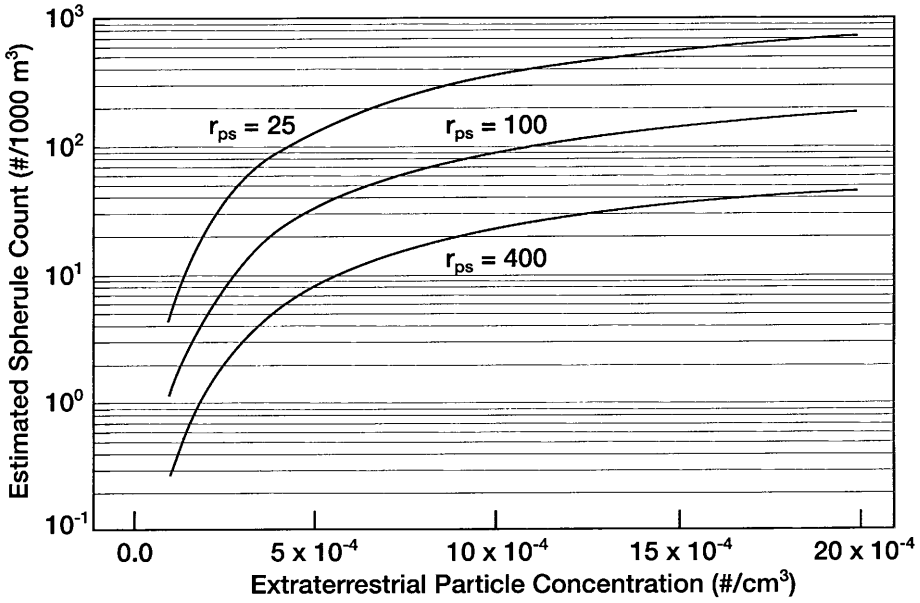

Fig. 6. – Estimated magnetic spherule sample count *vs.* extraterrestrial particle concentration in the ozone layer for three particle/spherule ratios ($r_{\rm ps} = 25$, 100, 400).

$W \equiv 1.81 \times 10^{-9}$ g/cm^3, water made available by condensation due to a 1 K drop in temperature in saturated air at 215 K,

$V_{\rm agg}$ is the particle aggregate terminal velocity (cm/s),

$R_{\rm agg}$ is the expected equivalent particle aggregate radius (cm).

Plots of $n_{\rm sph}$ *vs.* N for three values of $r_{\rm ps}$ are given in fig. 6.

Our extraterrestrial particle concentration estimate over South Pole is based on the following considerations:

– The ratio of the number of extraterrestrial particles to the number of magnetic spherules is taken to be 100 (sect. **3**).

– Magnetic spherule counts are assumed to range between 50 and 150 (sect. **4**). In fact, this range tends to overestimate counts for samples taken in the Northern Hemisphere [3] but underestimate counts for samples taken in the Southern Hemisphere [6].

– The geometrical enhancement of relative flux depicted in fig. 4 argues in favor of higher particle concentrations at South Pole, at least for southern streams of slow to moderate speed.

– Deviation from isokinetic sampling for larger particles, and particle aggregates in particular, also argues in favor of higher particle concentrations.

According to fig. 6, magnetic spherule counts of 50, 100, and 150 correspond to extraterrestrial particle concentrations in the ozone layer of 6.6×10^{-4}, 1.1×10^{-3}, and 1.7×10^{-3} cm^{-3}.

We shall assume in Part II of this paper that the concentration of extraterrestrial particles in the ozone layer over South Pole during ozone hole formation lies between 500 and 2000/m^3.

Appendix A.

Extraterrestrial particle aggregation

The object of this appendix is to derive an estimate for the concentration of extraterrestrial particles in the ozone layer in terms of magnetic spherule counts in air samples at ground level. This estimate is based on a model in which extraterrestrial particles settle rapidly through the atmosphere to about 30 km altitude. Settling slows appreciably between 20 and 30 km because of increasing atmospheric density. Absorption of solar radiation by ozone in this layer causes the air temperature to cycle diurnally [12]. During intervals of lowest temperature, water vapor in excess of saturation condenses on these particles to form ice crystals. This population evolves according to the coalescence equation [13]. Ice crystal aggregates that exceed a critical mass precipitate out of this layer. During their descent from 20 to 10 km, the ice sublimates to yield loosely bound particle aggregates. The resolution of features in fig. 2 implies the descent of these aggregates from 10 to 0 km takes on the order of 24 h.

Given this model, we estimate the concentration of extraterrestrial particles in the ozone layer in three steps. The first is to specify the coalescence equation for the evolution of ice crystal aggregates. The second is to derive an equation relating the concentration of precipitating ice crystal aggregates between 20 and 30 km and the expected number of magnetic spherules in an air sample at ground level. The third is to integrate these equations using values of parameters inferred from available data. The results are given in fig. 6.

To derive the coalescence equation for ice crystal aggregates, take

$f(u)\delta u$ is the number of aggregates (#/cm^3) with masses in the interval $[u, u+\delta u]$,

$g(u)\delta u$ is the number of precipitating aggregates (#/cm^3) with masses in the interval $[u, u+\delta u]$,

$K(u,v)$ is the coalescence kernel for aggregates with masses u and v (cm^3/s),

$V(u)$ is the terminal velocity of an aggregate with mass u (cm/s),

$R(u)$ is the effective radius (cm) of an aggregate with mass u,

L is the minimum mass of precipitating aggregates (g).

The collision rate (#/s) between a given ice crystal aggregate with mass u and aggregates with masses in the interval $[v, v+\delta v]$ is

$$K(u,v)f(v)\delta v \approx \pi \left(R(u)+R(v)\right)^2 |V(u)-V(v)| f(v)\delta v.$$

The collision rate (#/cm^3/s) between aggregates with masses in the intervals $[u, u+\delta u]$ and $[v, v+\delta v]$ is

$$\frac{1}{2}K(u,v)f(u)f(v)\delta u\delta v.$$

Assuming that colliding aggregates coalesce [11], the rate at which aggregates enter the $[u, u+\delta u]$ mass interval (#/cm^3/s) is

$$\frac{1}{2}\int_0^u K(u-v,v)f(u-v)f(v)\mathrm{d}v\delta u,$$

and the rate at which crystals depart the interval is

$$f(u)\delta u\int_0^\infty K(u,v)f(v)\mathrm{d}v.$$

On balance,

$$\frac{\mathrm{d}f}{\mathrm{d}t}(u) = \frac{1}{2}\int_0^u K(u-v,v)f(u-v)f(v)\mathrm{d}v - f(u)\int_0^\infty K(u,v)f(v)\mathrm{d}v.$$

We assume that once an aggregate exceeds a given critical size L, it exits the coalescence layer under the influence of gravity. Thus, the evolution of f is capped at L:

$$\frac{\mathrm{d}f}{\mathrm{d}t}(u) = \frac{1}{2}\int_0^u K(u-v,v)f(u-v)f(v)\mathrm{d}v - f(u)\int_0^L K(u,v)f(v)\mathrm{d}v \tag{A.1}$$

for $u \leqslant L$, and $f(u) \equiv 0$ for $u > L$. The equation for g is derived similarly:

$$\frac{\mathrm{d}g}{\mathrm{d}t}(u) = \frac{1}{2}\int_0^u K(u-v,v)f(u-v)f(v)\mathrm{d}v \tag{A.2}$$

for $u > L$, and $g(u) \equiv 0$ for $u \leqslant L$.

The first factor in the coalescence kernel is just the collision cross-section for two spheres falling along strictly rectilinear trajectories. The expression for terminal velocity in the second factor is Oseen's extension of Stokes' formula [11]. In this case, the coefficient of drag is given by

$$C_\mathrm{D} = \frac{24}{\mathrm{Re}}\left(1 + \frac{3}{16}\mathrm{Re}\right),$$

where

$\mathrm{Re} = 2\rho_\mathrm{a}\mathrm{RV}/\mu$ (Reynolds number),

ρ_a is the density of air ($\sim 4\times10^{-5}$ g/cm^3 at 25 km altitude),

μ is the coefficient of viscosity (1.42×10^{-5} g/cm/s).

Equating drag and gravitational forces on the crystal, we obtain

$$C_\mathrm{D}\left(\frac{1}{2}\rho_\mathrm{a}V^2\right)(\pi R^2) = \frac{4}{3}\pi R^3\rho_\mathrm{i}\tilde{g},$$

where

ρ_i is the density of ice (1.0 g/cm^3),

$\tilde{g}$ is the gravitational acceleration (980 cm/s/s).

Simplifying, we obtain

$$\frac{3}{8}\frac{\rho_{\mathrm{a}}}{\mu}RV^2 + V - \frac{2}{9}\frac{\rho_{\mathrm{i}}\tilde{g}}{\mu}R^2 = 0\,. \tag{A.3}$$

The equation is quadratic in both R and V. An expression for one variable in terms of the other is easily obtained using the quadratic formula.

For simplicity, we have assumed that the initial ice crystal population forms according to the following constraints. Crystals form on particles by ice nucleation followed by condensation. The time for crystals to fully form is negligible compared with the time for the population to evolve through coalescence. Each crystal contains (exactly) one particle. The size of a crystal is independent of the size of the particle on which it forms. Finally, the crystal formed on a given particle has mass proportional to the volume of the largest sphere centered at the particle that does not contain any other particles (at some snapshot in time).

Take

$f_0(u)\delta u$ = initial number of ice crystals (#/cm^3) with masses in the interval $[u, u+\delta u]$,

N = number density of particles (#/cm^3),

W = water vapor available for ice crystal formation (g/cm^3),

$\bar{u} \equiv W/N$, average initial ice crystal mass (g).

Assuming a uniform random distribution of particles, then the probability that no particles lie in a thin spherical shell centered on any given particle is $1 - N4\pi r^2\delta r$, where r is the radius of the shell and δr is its thickness. The probability $P(r)$ that no other particles lie in the sphere of radius r centered on the given particle is approximately

$$\prod_{i=1}^{n}\left(1 - N4\pi\left(ir/n\right)^2\left(r/n\right)\right),$$

where we have taken the sphere to be the union of n concentric thin shells. In the limit of large n,

$$\begin{aligned}
\ln P\left(r\right) &\approx \ln\prod_{i=1}^{n}\left(1 - N4\pi\left(ir/n\right)^2\left(r/n\right)\right)\\
&= \sum_{i=1}^{n}\ln\left(1 - N4\pi\left(ir/n\right)^2\left(r/n\right)\right)\\
&\approx -4\pi r^3 N\sum_{i=1}^{n}\left(\frac{i}{n}\right)^2\frac{1}{n}\\
&\to -4\pi r^3 N\int_0^1 s^2\mathrm{d}s\\
&= -\frac{4}{3}\pi r^3 N.
\end{aligned}$$

Thus,

$$P(r) = \exp\left[-\frac{4}{3}\pi r^3 N\right] .$$

The probability that a crystal in the initial population incorporates water vapor from a spherical volume with radius greater than r is $P\{\text{rad} > r\} = P(r)$. Thus, the probability that the corresponding volume is less than or equal to $\tilde{v}$ is $P\{\text{vol} \leqslant \tilde{v}\} = 1 - \exp[-N\tilde{v}]$. Finally, the probability that the mass of the corresponding ice crystal is less than or equal to u is $P\{\text{mass} \leqslant u\} = 1 - \exp[-(N/W)u]$. Thus, f_0 is exponential:

$$f_0(u)\,\delta u = N\frac{\mathrm{d}P}{\mathrm{d}u}\{\text{mass} \leqslant u\}\delta u = \frac{N^2}{W}\exp[-(N/W)u]\delta u\,. \tag{A.4}$$

The second step is to derive an equation relating the concentration of precipitating ice crystal aggregates between 20 and 30 km and the expected number of magnetic spherules in an air sample at ground level. We begin by deriving an estimate for L. Take

D_c = thickness of the coalescence layer, *i.e.*, the layer between 20 and 30 km altitude (10^6 cm),

D_g = thickness of the ground layer, *i.e.*, the layer between 0 and 10 km altitude (10^6 cm),

T = time for the smallest precipitating particle aggregates to settle through the ground layer (s),

R_{prt} = average particle radius ($\sim 5 \times 10^{-4}$ cm),

R_{agg} = expected particle aggregate equivalent radius (cm),

V_{agg} = particle aggregate terminal velocity (cm/s),

ρ_{prt} = particle density ($\sim$3.5 g/cm^3),

ρ_{agg} = particle aggregate density ($\sim$3.0 g/cm^3),

n_{prt} = expected number of particles in an aggregate,

n_{sph} = expected number of magnetic spherules in a daily air sample at ground level (#/sample),

V_{smp} = sample volume (10^9 cm^3),

r_{ps} = ratio of the number of extraterrestrial particles to number of magnetic spherules ($\sim$100).

First, we take $V_{agg} = D_g/T$. Next, given V_{agg}, ρ_{agg}, and ρ_a ($\sim 8.0 \times 10^{-4}$ g/cm^3 at 5 km), we obtain R_{agg} from eq. (A.3). Then n_{prt} satisfies

$$n_{prt}\frac{4}{3}\pi\left(R_{prt}\right)^3\rho_{prt} = \frac{4}{3}\pi\left(R_{agg}\right)^3\rho_{agg},$$

so

$$n_{prt} = \left(\frac{R_{agg}}{R_{prt}}\right)^3\frac{\rho_{agg}}{\rho_{prt}}.$$

Then our estimate for the minimum expected mass for precipitating ice crystal aggregates is

$$L = n_{\rm prt}\bar{u} = \left(\frac{R_{\rm agg}\left(D_{\rm g}/T, \rho_{\rm agg}, \rho_{\rm a}\right)}{R_{\rm prt}}\right)^3 \frac{\rho_{\rm agg} W}{\rho_{\rm prt} N}\,. \tag{A.5}$$

Given this estimate for L, we then solve the coalescence equation for g. The precipitation rate for ice crystal aggregates with masses in the interval $[u, u+\delta u]$ is $D_{\rm c} g(u)\delta u/8.64\times 10^4$ (#/cm^2/s), where the denominator is simply the number of seconds in a day. This precipitation rate equals the flux of corresponding particle aggregates at ground level. The expected number of particles in these aggregates is $u/\bar{u}$. The equivalent radius of the particle aggregates satisfies

$$\frac{u}{\bar{u}}\frac{4}{3}\pi\left(R_{\rm prt}\right)^3\rho_{\rm prt} = \frac{4}{3}\pi\left(R_{\rm agg}\right)^3\rho_{\rm agg},$$

so

$$R_{\rm agg} = R_{\rm prt}\left(\frac{\rho_{\rm prt} N}{\rho_{\rm agg} W} u\right)^{1/3}\,. \tag{A.6}$$

Terminal velocity $V_{\rm agg}(R_{\rm agg}(u), \rho_{\rm agg}, \rho_{\rm a})$ is obtained through eq. (A.3). The contribution to total particle aggregate number density at ground level is

$$\frac{D_{\rm c} g(u)\delta u}{8.64\times 10^4 V_{\rm agg}(R_{\rm agg}(u))}.$$

Finally, the expected number of spherules in a daily sample is

$$\begin{aligned} n_{\rm sph} &= \int_L^\infty \frac{V_{\rm smp}}{8.64\times 10^4}\frac{D_{\rm c} g(u)}{V_{\rm agg}(R_{\rm agg}(u))}\frac{n_{\rm prt}(u)}{r_{\rm ps}}{\rm d}u \\ &= \frac{V_{\rm smp} D_{\rm c} N}{8.64\times 10^4 r_{\rm ps} W}\int_L^\infty \frac{u g(u)}{V_{\rm agg}(R_{\rm agg}(u))}{\rm d}u\,. \end{aligned} \tag{A.7}$$

The final step in this development is to integrate these equations using values of parameters inferred from available data. We take $R_{\rm prt} = 5\times 10^{-4}$ cm and $r_{\rm ps} = 100$ based on measurements cited in sect. **3**. We infer that $T \sim 24$ h based on the resolution of features evident in fig. 2. N is an independent variable with a wide range of possible values. Finally, to estimate W, we consider the Clausius-Clapeyron equation for equilibrium water vapor density over an ice surface [17]:

$$\rho_{\rm e}\left(T_{\rm s}\right) = \rho_{\rm e}\left(T_0\right)\frac{T_0}{T_{\rm s}}\,\exp\left[\frac{M L_{\rm i}}{R}\cdot\left(\frac{1}{T_0}-\frac{1}{T_{\rm s}}\right)\right],$$

where

$\rho_{\rm e}$ is the equilibrium water vapor density over an ice surface (g/cm^3),

$T_{\rm s}$ is the ozone layer air temperature (215 K) [12],

T_0 is the reference air temperature (273 K),

$\rho_e(T_0) = 4.98 \times 10^{-6}$ g/cm^3,

M is the molecular weight of water (18 g/mole),

L_i is the latent heat of sublimation for ice (2825 J/g),

R is the gas constant (8.3144 J/K/mole).

We take $W \equiv \rho_e(T_s) - \rho_e(T_s - 1)$, *i.e.*, water made available through condensation due to a 1° drop in temperature in saturated air at T_s.

Given these parametric values, we then use eqs. (A.3) and (A.4) to evaluate the coalescence kernel K and the initial ice crystal distribution f_0. We then use eq. (A.5) to estimate the minimum mass L of precipitating aggregates. We solve eqs. (A.1) and (A.2) for the distribution g of precipitating ice crystal aggregates. Finally, given g, we use eqs. (A.3) and (A.6) to evaluate the integral in eq. (A.7) for n_{sph}. We have solved this system (numerically) for n_{sph} *vs.* N. The results are given in fig. 6.

Appendix B.

Relative extraterrestrial particle flux

The instantaneous flux F (#/cm^2/s) produced by a given (homogeneous) extraterrestrial particle stream is a function of the stream's particle density, speed, and angle of entry in the atmosphere. The relative instantaneous flux RF above a given sampling station is taken to be the instantaneous flux above the station divided by the maximum instantaneous flux taken over the surface of the Earth. The relative flux $\overline{RF}$ is then taken to be RF averaged over a 24 h period. $\overline{RF}$ provides an estimate of the relative particle count at a sampling station as a function of the speed and radiant declination of the particle stream and the latitude of the station.

The object of this appendix is to derive an analytical expression for $\overline{RF}$. The starting point is the equation for the orbit of an extraterrestrial particle near the Earth [18]. The orbit is assumed to be hyperbolic. In planar polar coordinates (r, θ), the equation takes the form

$$\frac{1}{r} = -\frac{mK}{L^2} + A\cos(\theta - \theta_0),$$

where

r is the distance between the particle and the center of the Earth (cm),

m is the mass of the particle (g),

$K \equiv -GmM$,

G is the universal gravitational constant, 6.67×10^{-8} dyne ·cm^2/g^2,

M is the mass of the Earth, 5.98×10^{27} g,

L is the angular momentum of the particle (g·cm^2/s),

A is a parameter that characterizes the angle between the orbit asymptotes (cm^{-1}),

θ is the polar coordinate of the particle (radians),

θ_0 is a parameter that characterizes the orbit orientation (radians).

E and L are constants of the motion given by

$$E = mv_R^2/2 + K/R,$$

$$L = mbv_\infty = \sqrt{2mE}b,$$

where

E is the total energy of the particle (ergs),

v_R is the speed of the particle at the top of the atmosphere (cm/s),

R is the distance between the center of the Earth and the top of the atmosphere, 6.37×10^8 cm,

b is the Rutherford scattering parameter, *i.e.*, the distance between the center of the Earth and an orbit asymptote (cm),

v_∞ is the speed of the particle far from the Earth (cm/s).

Finally, A is given by

$$A = \sqrt{\frac{m^2K^2}{L^4} + \frac{2mE}{L^2}}.$$

The first step in this derivation is to reorient the particle's orbit so that its approach to Earth is parallel to the polar axis. Take θ_0 such that $\theta \approx 0$ for large r. Then

$$0 = -\frac{mK}{L^2} + A\cos\theta_0,$$

so

$$A\cos\theta_0 = \frac{mK}{L^2} = \frac{K}{2E}\frac{1}{b^2},$$

and

$$A\sin\theta_0 = A\left[1 - \left(\frac{mK}{AL^2}\right)^2\right]^{1/2} = \left[A^2 - \frac{m^2K^2}{L^4}\right]^{1/2} = \left[\frac{2mE}{L^2}\right]^{1/2} = \frac{1}{b}.$$

With this orientation, b and θ at the Earth's surface are related by

$$\begin{aligned}\frac{1}{R} &= -\frac{mK}{L^2} + A\cos\theta_0\cos\theta + A\sin\theta_0\sin\theta \\ &= -\frac{mK}{2mE}\frac{1}{b^2} + \frac{K}{2E}\frac{1}{b^2}\cos\theta + \frac{1}{b}\sin\theta,\end{aligned}$$

or

$$\alpha\sin\theta + \beta\cos\theta = \gamma\,, \tag{B.1}$$

where $\alpha \equiv bR$, $\beta \equiv KR/2E$, and $\gamma \equiv \beta + b^2$. Note that this equation is quadratic in b and has solution

$$b = \frac{R\sin\theta + \sqrt{R^2\sin^2\theta - 4\beta\,(1-\cos\theta)}}{2}, \tag{B.2}$$

an explicit expression for b as a function of $\sin\theta$ and $\cos\theta$.

The second step is to derive an expression for instantaneous particle flux F as a function of θ. Note that the area of the region on the Earth with polar angle between θ and $\theta + \delta\theta$ is $\sim 2\pi R^2 \sin\theta\delta\theta$. Let Φ_∞ denote particle flux in the stream far from Earth. Then the rate at which particles fall on this region is $\sim 2\pi b\delta b\Phi_\infty$, where b and $b + \delta b$ correspond to θ and $\theta + \delta\theta$ via eq. (B.1). The flux over a station with polar angle θ is

$$F\,(\theta) = \lim_{\delta b\to 0} \frac{2\pi b\delta b\Phi_\infty}{2\pi R^2\sin\theta\delta\theta} = \frac{b\Phi_\infty}{R^2\sin\theta\frac{\mathrm{d}\theta}{\mathrm{d}b}}.$$

To compute $\mathrm{d}\theta/\mathrm{d}b$, differentiate eq. (B.1):

$$\frac{\mathrm{d}\alpha}{\mathrm{d}b}\sin\theta + \alpha\cos\theta\frac{\mathrm{d}\theta}{\mathrm{d}b} - \beta\sin\theta\frac{\mathrm{d}\theta}{\mathrm{d}b} = \frac{\mathrm{d}\gamma}{\mathrm{d}b},$$

or

$$R\sin\theta + (\alpha\cos\theta - \beta\sin\theta)\frac{\mathrm{d}\theta}{\mathrm{d}b} = 2b.$$

Thus,

$$\frac{\mathrm{d}\theta}{\mathrm{d}b} = \frac{2b - R\sin\theta}{\alpha\cos\theta - \beta\sin\theta}.$$

Substituting,

$$F\,(\theta) = \frac{\Phi_\infty b}{R^2\sin\theta}\frac{\alpha\cos\theta - \beta\sin\theta}{2b - R\sin\theta}\,. \tag{B.3}$$

The third step is to compute an expression for relative instantaneous flux RF. By definition, $RF(\theta) \equiv F(\theta)/F(0)$, where $F(0) \equiv \lim_{\theta\to 0} F(\theta)$. To evaluate this limit, rewrite eq. (B.2) in the form

$$\frac{2b - R\sin\theta}{R\sin\theta} = \sqrt{\frac{R^2\sin^2\theta - 4\beta\,(1-\cos\theta)}{R^2\sin^2\theta}},$$

or

$$\frac{b/R}{\sin\theta} = \frac{1 + \sqrt{1 - \frac{4\beta}{R^2}\left(\frac{1-\cos\theta}{\sin^2\theta}\right)}}{2}.$$

Let ϕ denote the limit

$$\phi \equiv \lim_{\theta\to 0}\frac{b/R}{\sin\theta} = \lim_{\theta\to 0}\frac{1 + \sqrt{1 - \frac{4\beta}{R^2}\left(\frac{1-\cos\theta}{\sin^2\theta}\right)}}{2} = \frac{1 + \sqrt{1 - \frac{2\beta}{R^2}}}{2}\,. \tag{B.4}$$

Using this result to evaluate $F(0)$,

$$F(0) \equiv \lim_{\theta\to 0} F(\theta) = \lim_{\theta\to 0} \frac{\Phi_\infty}{R}\left(\frac{b/R}{\sin\theta}\right)\frac{R\cos\theta\left(\frac{b/R}{\sin\theta}\right)-\frac{\beta}{R}}{2\left(\frac{b/R}{\sin\theta}\right)-1} = \frac{\Phi_\infty}{R^2}\frac{\phi\left(R^2\phi-\beta\right)}{2\phi-1}.$$

Finally, the expression for relative instantaneous flux is given by

$$RF(\theta) \equiv F(\theta)/F(0) = \frac{2\phi-1}{\phi\left(R^2\phi-\beta\right)}\frac{b\left(bR\cos\theta-\beta\sin\theta\right)}{\sin\theta\left(2b-R\sin\theta\right)}. \tag{B.5}$$

The final step is to derive an expression for relative flux $\overline{RF}$. Let $\vec{R}$ denote the position vector for a sampling station and $\vec{v}_R$ the velocity vector for an extraterrestrial particle stream. To account for the dependence of $\vec{R}$ on time, take a coordinate system in which $\vec{R}$ and $\vec{v}_R$ have representations

$$\vec{R}(t) = (R\cos\lambda\cos\omega t, R\cos\lambda\sin\omega t, R\sin\lambda)$$

and

$$\vec{v}_R = -(v_R\cos\delta, 0, v_R\sin\delta),$$

where

λ is the latitude of the sampling station (radians),

ω is the angular velocity of the Earth (radians/s),

t is the time (s),

δ is the radiant declination of the particle stream (radians).

Then RF over the sampling station depends on time through the relation

$$\cos\theta(t) = \frac{-\vec{v}_R\cdot\vec{R}(t)}{v_R R} = \cos\delta\cos\lambda\cos\omega t + \sin\delta\sin\lambda. \tag{B.6}$$

Relative flux $\overline{RF}(\lambda,\delta,v_R)$ is simply $RF(\theta(t),v_R)$ averaged over a 24 h period T:

$$\overline{RF}(\lambda,\delta,v_R) = \frac{1}{T}\int_0^T RF(\theta(t),v_R)\mathrm{d}t,$$

where integrand is taken to be zero when the sampling station is in the shadow of the Earth.

To summarize, $b(t)$ and $\cos\theta(t)$ are given by eqs. (B.2) and (B.6). Relative instantaneous flux above a sampling station at latitude λ and time t is obtained by substituting these time-dependent expressions into eq. (B.5):

$$RF(t) = \frac{2\phi-1}{\phi\left(R^2\phi-\beta\right)}\frac{b(t)\left(b(t)R\cos\theta(t)-\beta\sin\theta(t)\right)}{\sin\theta(t)\left(2b(t)-R\sin\theta(t)\right)}. \tag{B.7}$$

Finally, relative flux $\overline{RF}$ for a station with latitude λ and shower with velocity v_R and declination δ is just the 24 h average

$$\overline{RF}\,(\lambda, v_R, \delta) = \frac{1}{T}\int_0^T RF\,(t)\mathrm{d}t\,. \tag{B.8}$$

Estimates based on this derivation are illustrated in fig. 4.

* * *

The authors wish to acknowledge the kind invitation by Prof. F. PRODI to the Physics Department of the University of Ferrara, Italy, preparation of figures by Mr. M. SHIBAO, National Center for Atmospheric Research (NCAR), Boulder, Colorado, USA, library services by Ms. L. FOREHAND (NCAR), the continual assistance and support of Dr. G. A. KRAS, M.D., and the patience of Mrs. D. KERRIGAN during the protracted distractions of her spouse.

REFERENCES

[1] BOWEN E. G., *The relation between rainfall and meteor showers*, *J. Met.*, **13** (1956) 142.
[2] WHIPPLE F. L. and HAWKINS G. S., *Encyclopaedia of Physics*, Vol. II, *Meteors* (Springer-Verlag, Berlin) 1959.
[3] ROSINSKI J., *Extraterrestrial magnetic spherules: their association with meteor showers and rainfall frequency*, *J. Atmos. Terr. Phys.*, **32** (1970) 805.
[4] ROSINSKI J., NAGAMOTO C. T. and BAYARD M., *Extraterrestrial particles and precipitation*, *J. Atmos. Terr. Phys.*, **37** (1975) 1231.
[5] SCHMIDT R. A., NASA Tech. Note No. D-2719, Washington, D.C., 1965.
[6] ROSINSKI J., *On the ozone hole in October*, *Nuovo Cimento*, **19** (1996) 417.
[7] ROSINSKI J., *Global deposition of extraterrestrial particles during October*, *J. Atmos. Terr. Phys.*, **34** (1972) 487.
[8] ROSINSKI J. and SNOW R. H., *Secondary particulate matter from meteor vapors*, *J. Met.*, **18** (1961) 736.
[9] KORNBLUM J. J., *Micrometeoroid interaction with the atmosphere*, *J. Geophys. Res.*, **74** (1969) 1893.
[10] ROSINSKI J., NAGAMOTO C. T. and KERRIGAN T. C., *Source of extraterrestrial spheroids*, *J. Atmos. Terr. Phys.*, **35** (1973) 95.
[11] FUCHS N. A., *The Mechanics of Aerosols* (Macmillan, New York, N.Y.) 1964.
[12] *Handbook of Geophysics* (Macmillan, New York, N.Y.) 1961.
[13] HIDY G. M. and BROCK J. R., *The Dynamics of Aerocolloidal Systems* (Pergamon, New York, N.Y.) 1970.
[14] ROSINSKI J., NAGAMOTO C. T., LANGER G. and PARUNGO F. P., *Cirrus clouds as collectors of aerosol particles*, *J. Geophys. Res.*, **75** (1970) 2961.
[15] *ALPO Meteor Shower List* (Association of Lunar and Planetary Observers, `www.lpl.arizona/~rhill/alpo`) 2000.
[16] KOMHYR W. D., OLTMANS S. J. and GRASS R. D., *Atmospheric ozone at South Pole, Antarctica, in 1986*, *J. Geophys. Res.*, **93** (1988) 5167.
[17] REIF F., *Fundamentals of Statistical and Thermal Physics* (McGraw-Hill, New York, N.Y.) 1965.
[18] SIMON K. R., *Mechanics* (Addison-Wesley, Reading, Massachusetts) 1960.